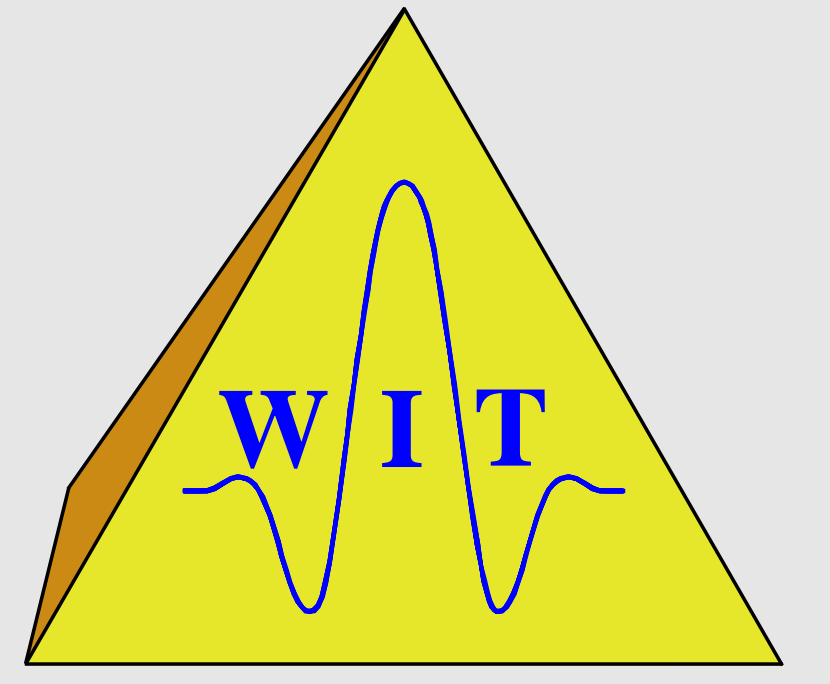


# Common-Reflection-Surface Stack and Conflicting Dips

Jürgen Mann

Geophysical Institute, University of Karlsruhe, Germany



## Summary

The common-reflection-surface (CRS) stack was introduced as a data-oriented method to simulate zero-offset (ZO) sections from multi-coverage seismic reflection data for 2-D media. The CRS stacking operator, parameterized by means of kinematic wavefield attributes, represents an analytic approximation of the kinematic reflection response of a curved reflector segment.

So far, the implemented CRS stack strategy was only able to determine one stacking operator for each ZO sample to be simulated. Thus, conflicting dip situations cannot be resolved. In this contribution, I introduce an extended CRS stack strategy that overcomes this limitation. The application of this extended strategy is discussed for a synthetic and a real data example.

## Basic task of the CRS stack

The main objective of the CRS stack method is to determine the analytic stacking operator that fits best an actual reflection event in the multi-coverage data. The hyperbolic approximation of the CRS stacking operator (Schleicher et al., 1993; Tygel et al., 1997) reads

$$t^2(x_m, h) = \left( t_0 + \frac{2 \sin \alpha (x_m - x_0)}{v_0} \right)^2 + \frac{2 t_0 \cos^2 \alpha}{v_0} \left( \frac{(x_m - x_0)^2}{R_N} + \frac{h^2}{R_{NIP}} \right), \quad (1)$$

where the midpoint  $x_m$  and the half-offset  $h$  of a shot/receiver pair represent the acquisition geometry. The ZO sample to be simulated is given by  $t_0$  and  $x_0$ ,  $v_0$  is the near-surface velocity.

The wavefield attributes  $\alpha$ ,  $R_{NIP}$ , and  $R_N$  are connected with the reflector segment's properties (location, orientation, curvature) by means of two hypothetical experiments, see Figure 1. A point source at  $R$  and an exploding reflector experiment yield wavefronts emerging with curvature  $R_{NIP}$  and  $R_N$  at  $x_0$ , respectively. The emergence angle of the normal ray is given by  $\alpha$ .

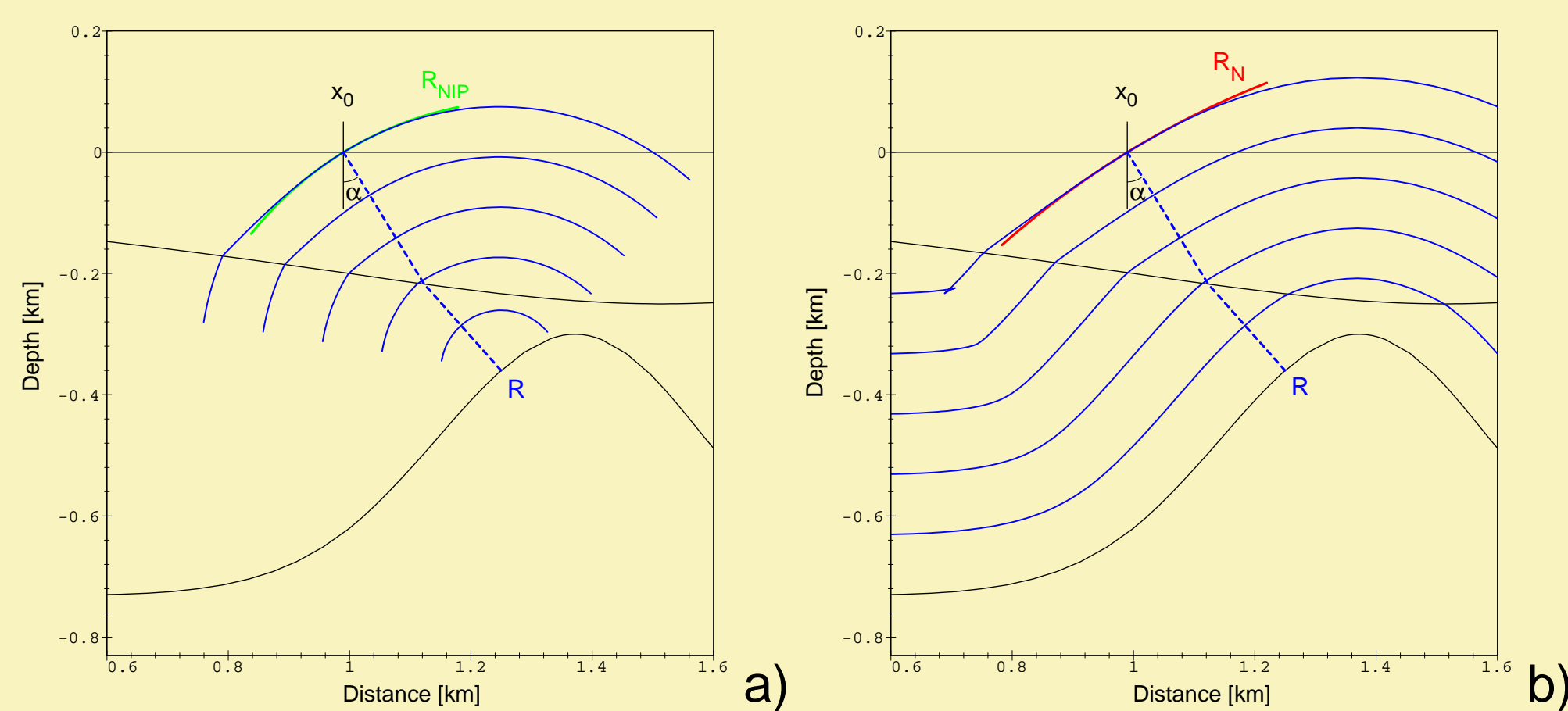


Figure 1: Two hypothetical experiments: a) a point source at  $R$  and b) an exploding reflector experiment yield wavefronts emerging with curvature  $R_{NIP}$  and  $R_N$  at  $x_0$ , respectively. The normal ray from  $R$  to  $x_0$  is depicted as a dashed blue line.

The optimum wavefield attributes  $\alpha$ ,  $R_{NIP}$ , and  $R_N$  are determined by means of coherence analysis. Thus, a global optimization problem with three parameters has to be solved. To consider conflicting dip situations, local coherence maxima have to be considered, too.

An actual global optimization with three parameters is extremely time consuming. Thus, we have to split the problem into separate simpler optimization steps.

## Pragmatic search strategy

Müller et al. (1998) and Müller (1998) proposed to determine initial values for the wavefield attributes in specific subsets of the multi-coverage data. With approximate initial wavefield attributes, a subsequent local optimization is sufficient to obtain the final, optimized, attributes. In the chosen subsets of the multi-coverage data, the CRS stacking operator reduces to hyperbolae with one or two parameters:

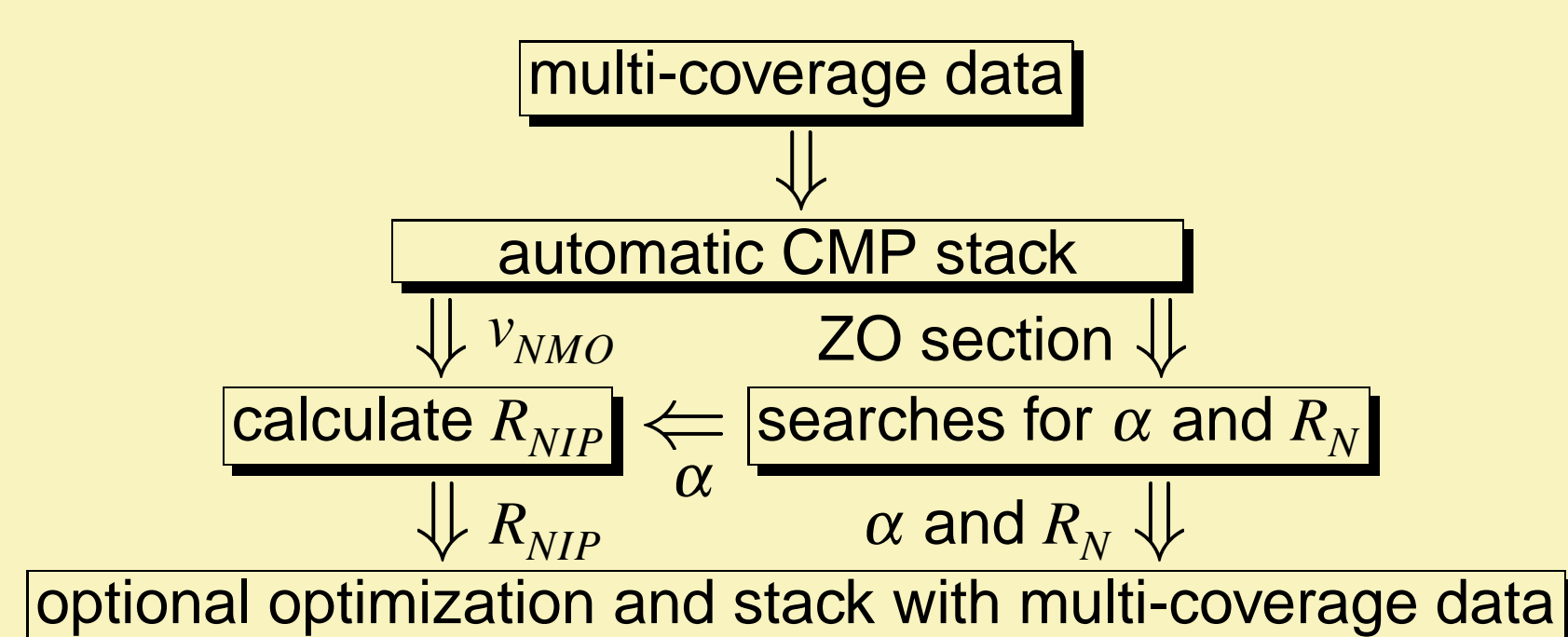
Common-midpoint (CMP) gather ( $x_m = x_0$ ):

$$t_{CMP}^2(h) = t_0^2 + \frac{4h^2}{v_{NMO}^2} \quad \text{with} \quad v_{NMO}^2 = \frac{2v_0 R_{NIP}}{t_0 \cos^2 \alpha} \quad (2)$$

Zero-offset section ( $h = 0$ ):

$$t_{ZO}^2(x_m) = \left( t_0 + \frac{2 \sin \alpha (x_m - x_0)}{v_0} \right)^2 + \frac{2 t_0 \cos^2 \alpha (x_m - x_0)^2}{v_0 R_N} \quad (3)$$

The details of this pragmatic search strategy can, e.g., be found in Mann et al. (1999) and Jäger et al. (2001). In this context, I only refer to a simplified flowchart of this strategy:



## Detection of conflicting dips

With the pragmatic search strategy, only one stacking operator is assigned to each ZO sample to be simulated. In case of conflicting dip situations, the less coherent event(s) will be suppressed. Furthermore, the stacking velocity  $v_{NMO}$  determined at such locations does not accurately correspond to the most coherent event, but might be affected by the conflicting event(s), too.

The first step of the pragmatic strategy, the automatic CMP stack, is not suited to separate conflicting dips, as the contributing events might be associated with similar stacking velocities.

Although conflicting dip situations are not considered in the automatic CMP stack, they can still be detected in the CMP stacked section. Three events with different dips can be identified in the angle spectrum in Figure 2. This spectrum was computed for a ZO location where two diffraction patterns (at  $\alpha \approx -30^\circ$  and  $\alpha \approx 25^\circ$ , respectively) and a weak reflection event (at  $\alpha \approx 12^\circ$ ) intersect each other.

With appropriate coherence thresholds, a discrete number of contributing events with different emergence angles can be determined. The emergence angles, in turn, are directly related to the dips of the events.

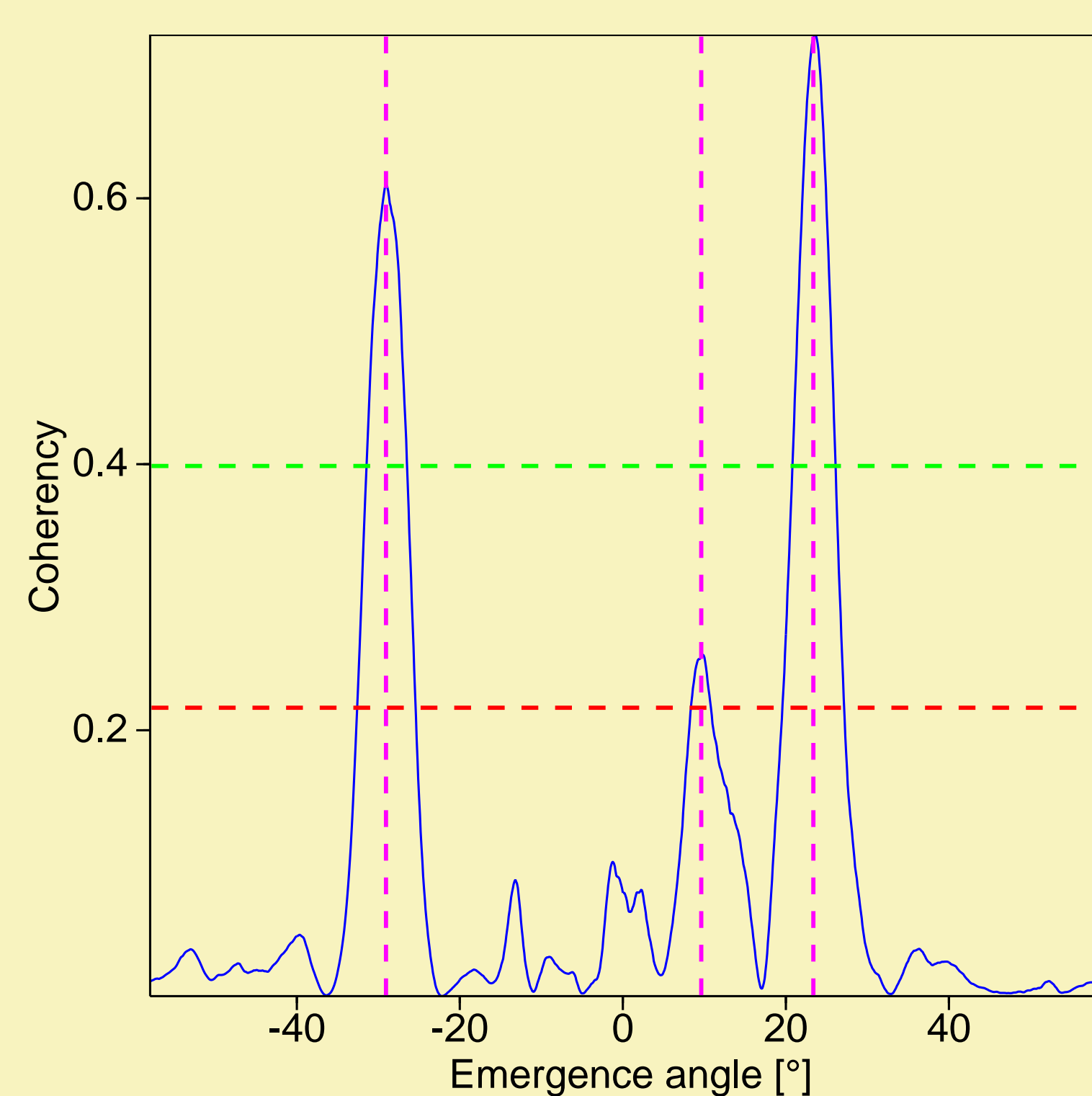


Figure 2: Angle spectrum for a ZO sample with three conflicting events. By applying appropriate absolute and relative thresholds, the emergence angles can be detected for all contributing events.

Thus, the pragmatic search strategy can be easily extended to detect conflicting dip situations and to determine the wavefield attributes  $\alpha$  and  $R_N$  in the CMP stacked section separately for each contributing event.

However, it is no longer possible to calculate  $R_{NIP}$  from  $\alpha$  and  $v_{NMO}$ : in general, I obtain an entire set of emergence angles  $\alpha^{(i)}$  but only one stacking velocity  $v_{NMO}$ . Obviously, an additional search procedure for  $R_{NIP}$  is now required to resolve this ambiguity.

## Determination of $R_{NIP}$

In view of the good performance of the pragmatic search strategy based on the processing of subsets of the multi-coverage data, it suggests itself to use a similar strategy to determine  $R_{NIP}$ . However, considering Equations (2) and (3), I observe that none of the subsets used so far is suited for this task: in the ZO section,  $R_{NIP}$  does not contribute, and in the CMP gather,  $\alpha$  and  $R_{NIP}$  cannot be separated.

I propose to use another subset of the multi-coverage data, namely the common-shot (CS) and the common-receiver (CR) gather defined by  $|x_m - x_0| = |h|$ . Here, the stacking operator (1) reduces to

$$t_{CS}^2(x_m) = \left( t_0 + \frac{2 \sin \alpha (x_m - x_0)}{v_0} \right)^2 + \frac{2 t_0 \cos^2 \alpha (x_m - x_0)^2}{v_0 R_{CS}}, \quad (4)$$

with  $1/R_{CS} = 1/R_{NIP} + 1/R_N$ . As  $\alpha$  and  $R_N$  are already determined, this implies a one parameter search in this gather.

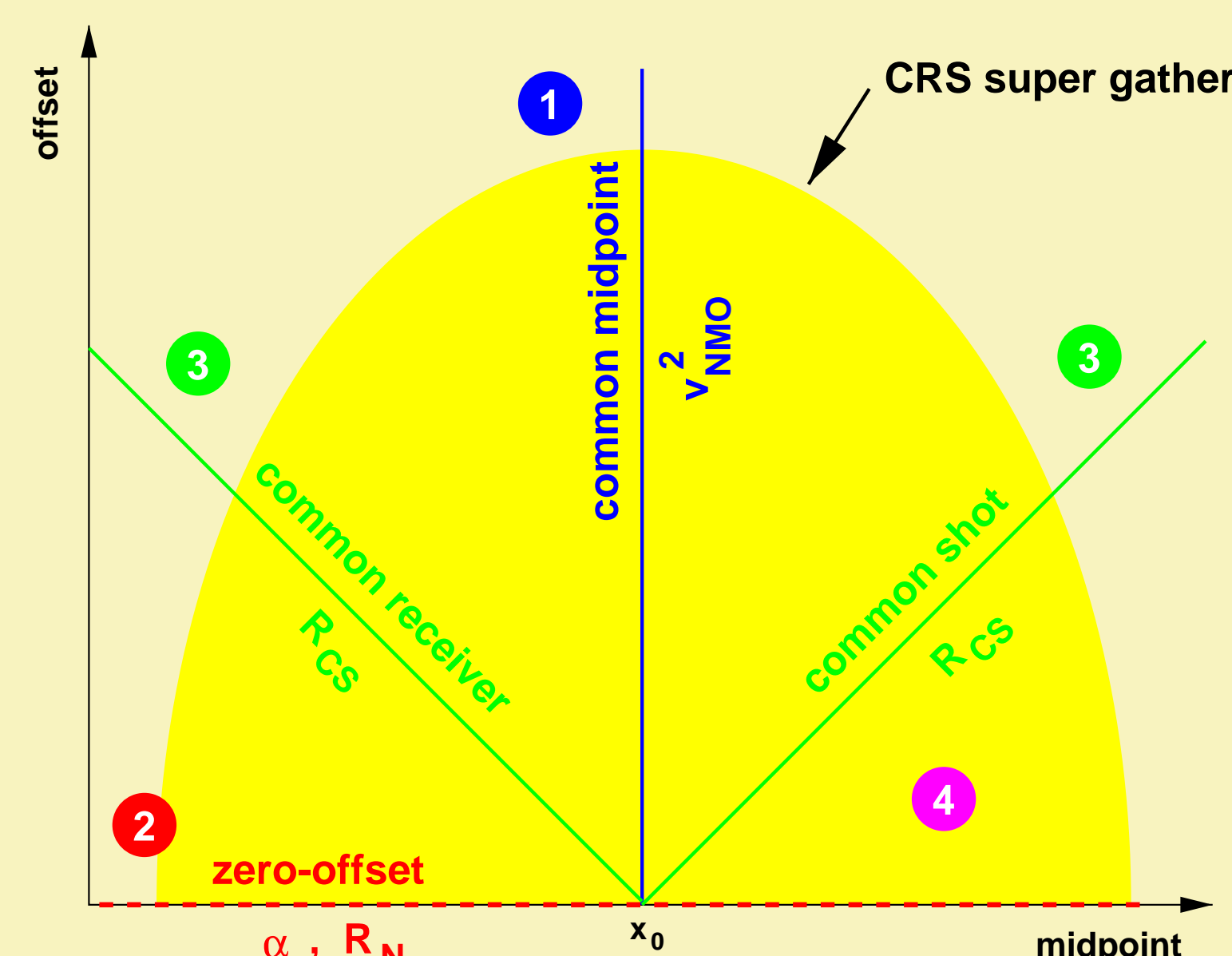


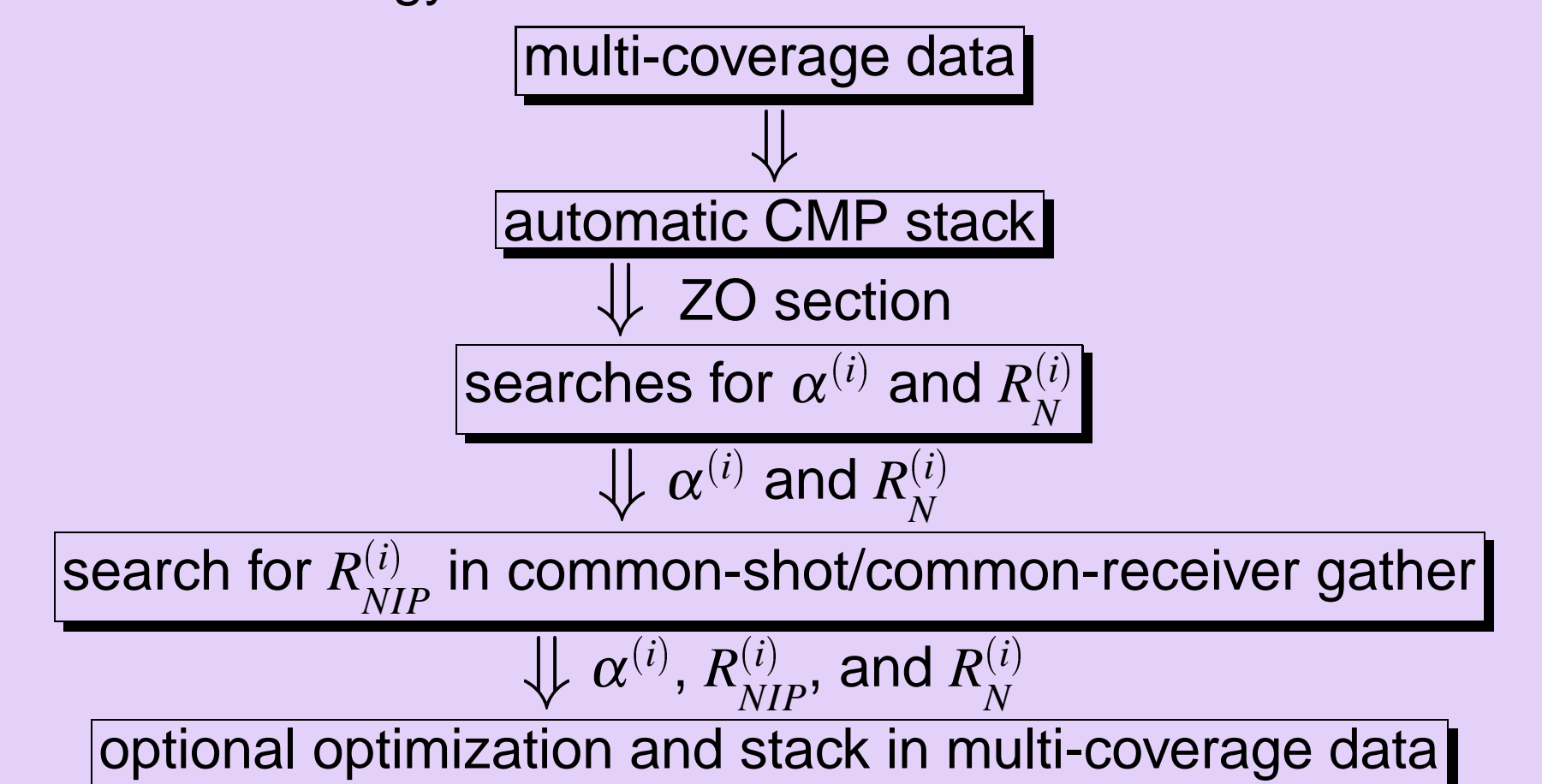
Figure 3: Used subsets of the multi-coverage data and their corresponding wavefield attribute(s). The numbers indicate the order of application of the corresponding processing steps.

## Extended search strategy

To set up an extended search strategy for conflicting dip situations, I summarize the above observations. In the following, the index  $i$  denotes the  $i$ th event detected for a particular ZO sample to be simulated.

- Conflicting dip situations can be easily identified in a ZO section. A CMP stacked section is well suited for this task.
- The emergence angles  $\alpha^{(i)}$  and the radii of curvature  $R_N^{(i)}$  can be detected in the CMP stacked section.
- An additional search for the radii of curvature  $R_{NIP}^{(i)}$  can be (indirectly) performed in the CS/CR gather.
- If only one event is found, the pragmatic search strategy is sufficient and the additional search can be omitted.

The extended strategy can be summarized as follows:



This extended search strategy requires only little additional effort compared to the pragmatic approach:

- The identification of conflicting dip situations is very fast, as no additional coherence analysis is required.
- An additional coherence analysis only has to be performed at ZO locations where conflicting dips are actually detected.
- Relevant conflicting dip situations usually only cover a small part of the ZO section to be simulated.

## Extended CRS stack vs. NMO/DMO/stack

Conflicting dip situations are usually resolved by applying a normal moveout (NMO) correction followed by a dip moveout (DMO) correction and stack. If performed in a single step, this process is also called migration to zero-offset (MZO).

Although the aim of the NMO/DMO/stack and the extended CRS stack—the simulation of a ZO section—is the same, there are substantial differences between both methods:

NMO/DMO/stack:

- Operator based on ZO isochron segment
- Summation of all possible contributing dips
- Correct DMO operator requires velocity model
- DMO provides no additional information

Extended CRS stack:

- Operator based on arbitrarily curved reflector segment
- Discrete number of contributing dips
- Data-oriented, a priori model is optional
- Separate wavefield attributes for each detected dip

Due to its more general model assumption, the CRS stacking operator is considerably larger than the DMO or MZO operator (see Figure 4). Thus, the CRS stack makes more extensive use of the redundancy in the multi-coverage data. Furthermore, each detected contributing event is handled completely separately.

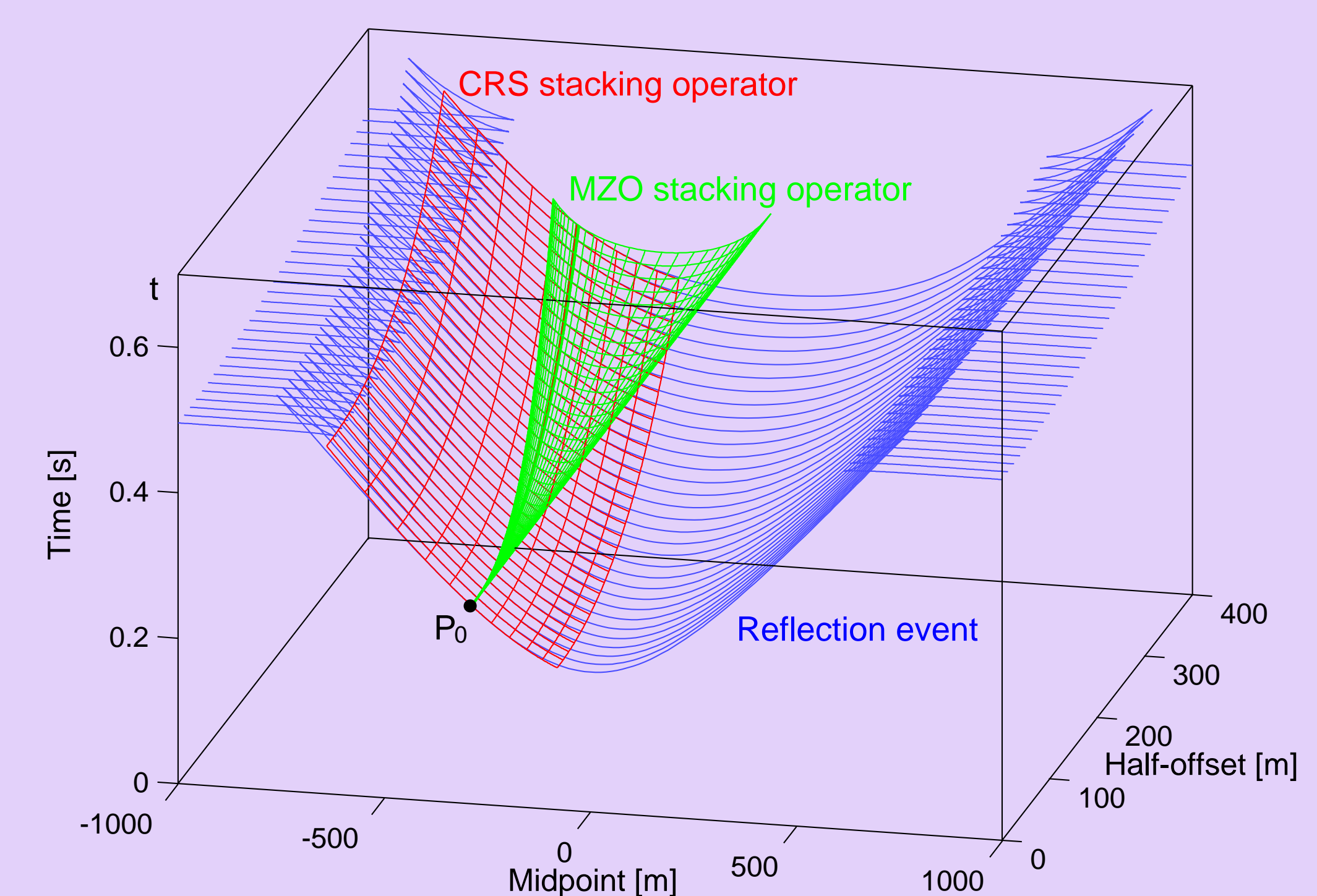


Figure 4: Comparison of the MZO stacking operator (green) and the CRS stacking operator (red) for the ZO location  $P_0$ . The blue lines represent the actual reflection event forward-calculated by means of ray tracing. The CRS stacking operator fits much closer to the reflection event.

## Synthetic example: Sigsbee 2A data

The marine Sigsbee 2A data set was simulated by the *Subsalt Multiples Attenuation and Reduction Technologies* (SMART) oil industry joint venture by means of a finite difference approximation of the acoustic wave equation. Although the model was not distributed with the pre-stack data, the CRS stack results indicate a salt cushion of complex shape embedded in a stratified medium. Furthermore, the model obviously contains two rows of diffraction points that cause conflicting dips situations. In Figures 5 and 6 subsets of the CRS stack results are shown obtained with the pragmatic and the extended CRS stack strategy, respectively.

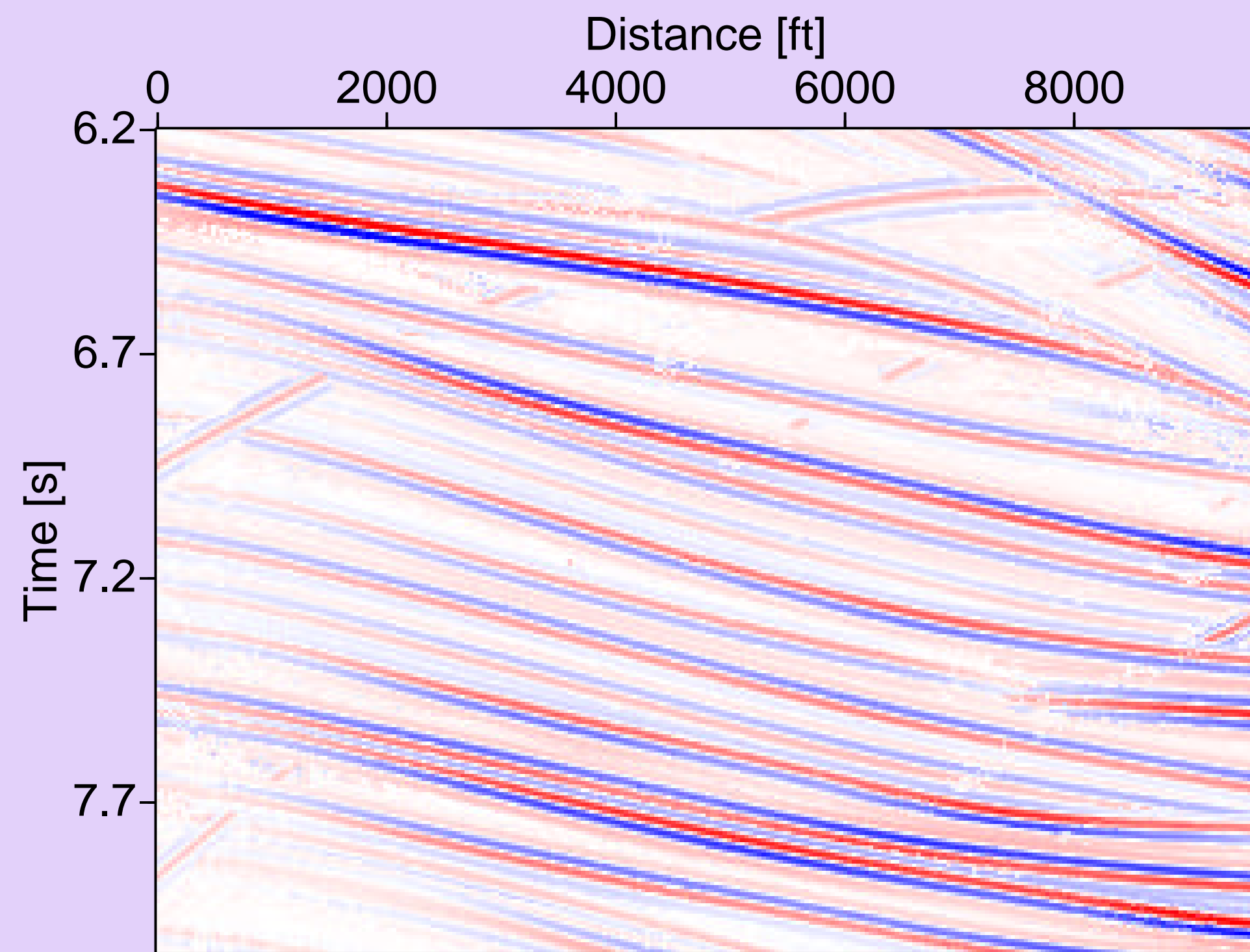


Figure 5: ZO section simulated with the pragmatic strategy. The steep diffraction events are suppressed at many locations.

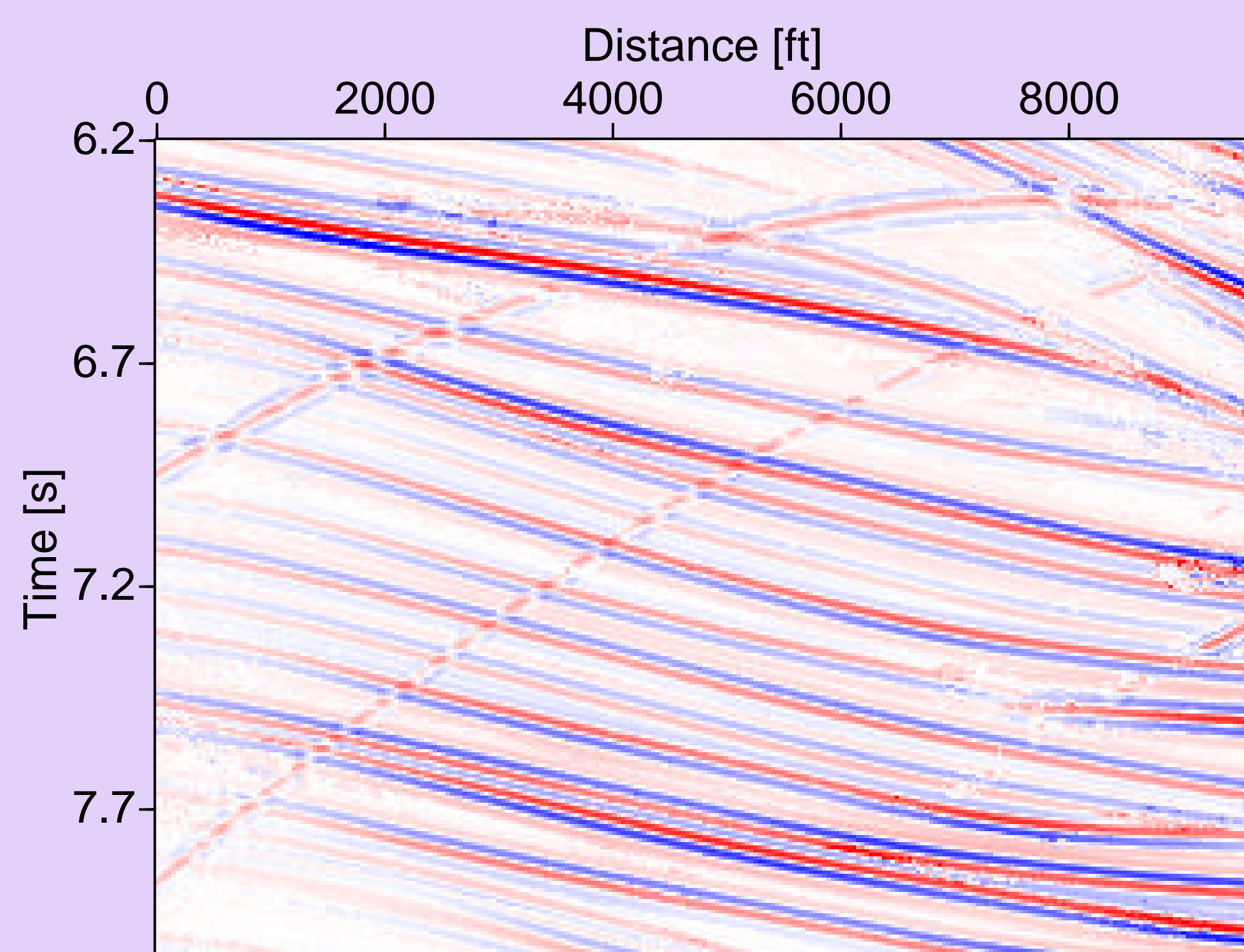


Figure 6: ZO section simulated with the extended strategy. The interference of conflicting events is simulated along the steep events.

The interfering events are separately characterized by means of different sets of wavefield attributes. As an example, the emergence angles are displayed in Figure 7. To preserve the spatial context, both sections are set to identical values at locations where only one dip is detected.

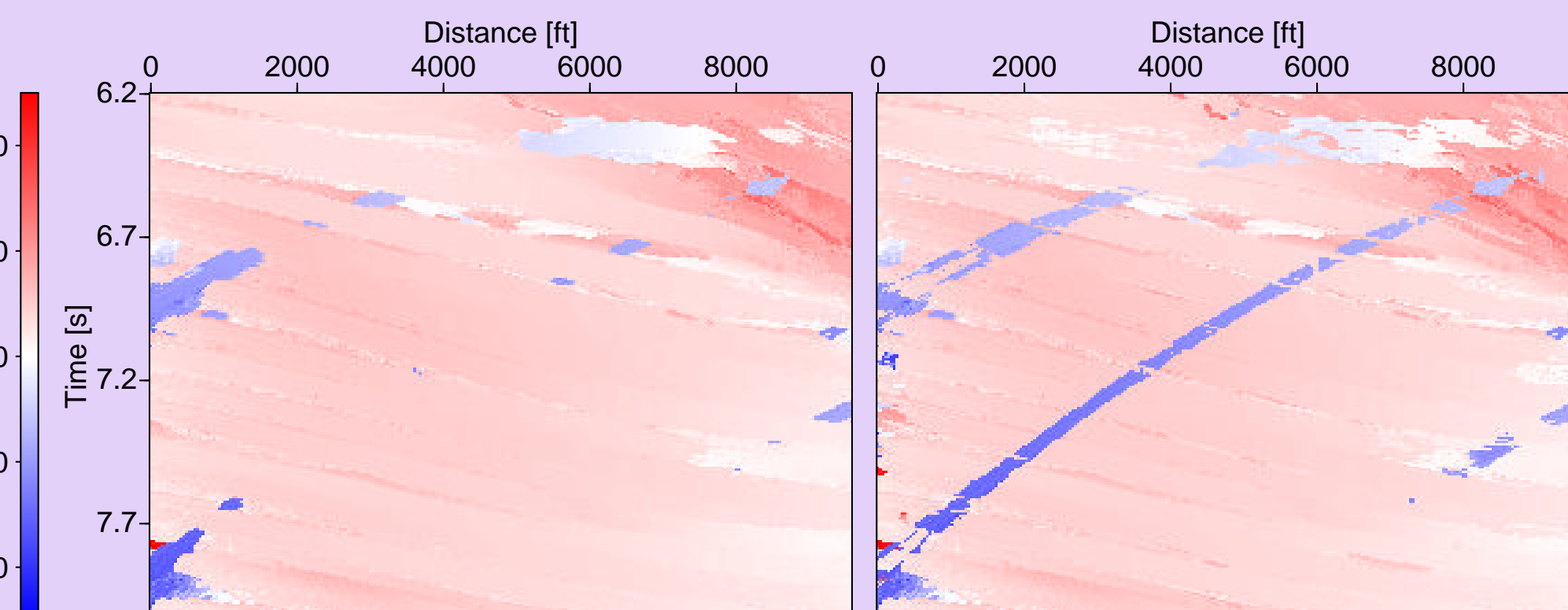


Figure 7: Emergence angles  $\alpha$  [°] of the events with the highest (left) and the second highest (right) coherence.

The attributes associated with one and the same event appear distributed over both sections of Figure 7. This is only a matter of data handling and does not affect the stack result.

For this example with diffraction patterns, an application of the remaining attributes  $R_{NIP}$  and  $R_N$  can be used to check the accuracy of the detected attributes: according to the hypothetical experiments shown in Figure 1, both wavefront curvatures should coincide for a diffraction. The ratio of both curvatures is depicted in Figure 8. The diffraction patterns can be clearly identified by means of the expected ratio 1. Again, they are distributed over both sections.

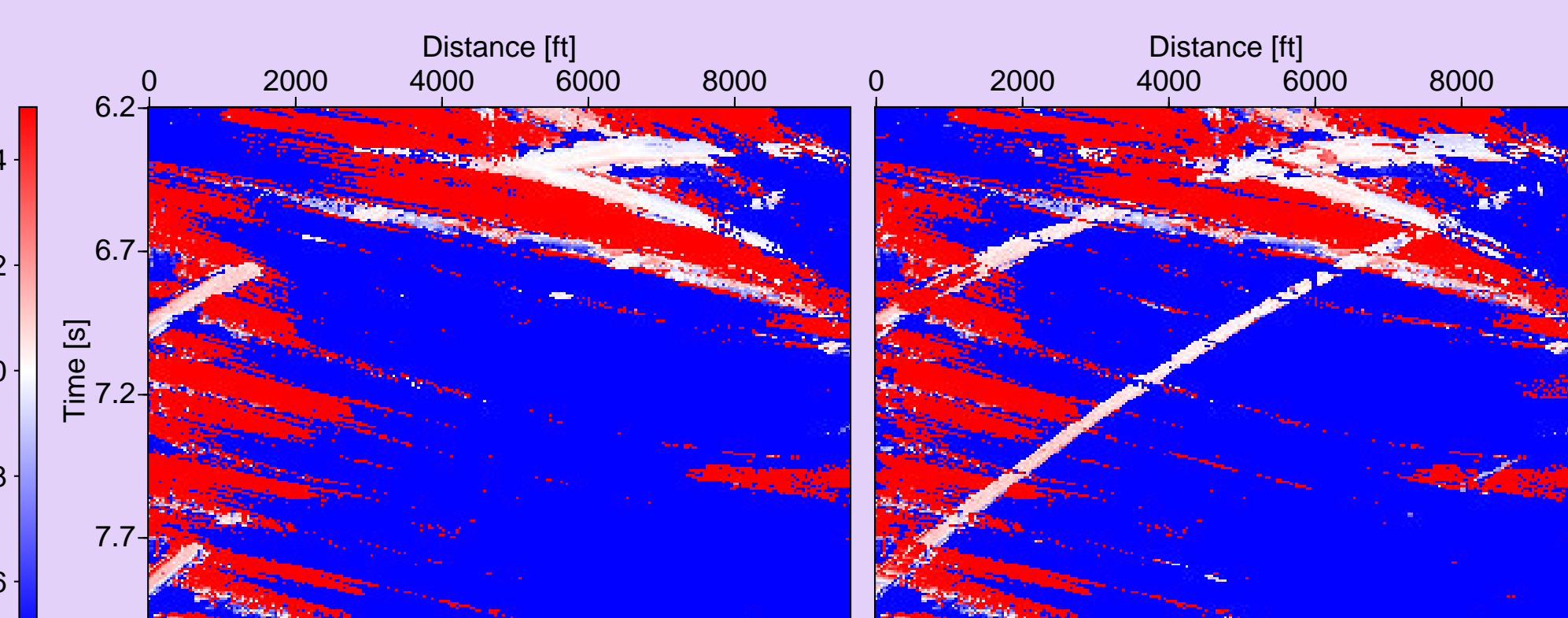


Figure 8: Ratio  $R_N/R_{NIP}$  of the events with the highest (left) and the second highest (right) coherence. As expected, the diffraction patterns are associated with a ratio close to 1.

For this synthetic example, the extended CRS stack strategy resolves most of the conflicting dip situations and yields reasonable attributes. The interference of conflicting events is well simulated.

## Real example: BGR99-07 data

The marine data set BGR99-07 was acquired in 1999 by the vessel *Prof. Polshkov* off-shore Costa Rica. The location is displayed in Figure 9. The data were provided by the *Federal Institute for Geosciences and Natural Resources* (BGR), Germany.

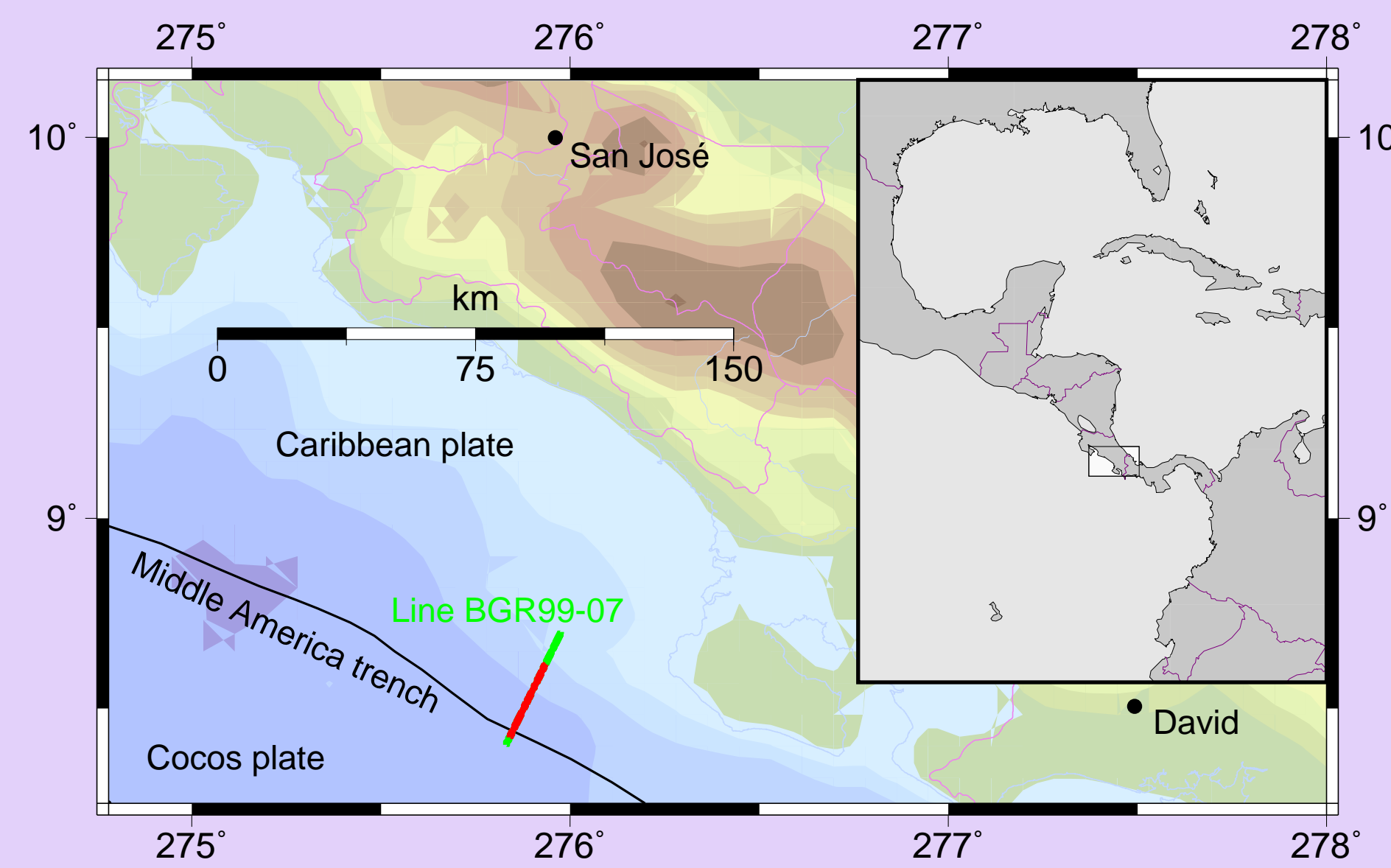


Figure 9: Location of acquisition. The subset of the acquired data processed with the CRS stack is shown in red.

The data set was recorded with a 360 channel streamer and a receiver interval of 12.5 m. The shot interval is 50 m with a total number of 480 shots. With a CMP bin spacing of 6.25 m the maximum fold is 49. Temporal sampling rate: 4 ms.

To test the extended search strategy under rather complicated conditions, I selected a detail with a steep event intersecting a low frequency event stemming from the boundary between the Cocos and the Caribbean plate. Figure 10 shows the near-offset traces extracted from the pre-stack data. The plate boundary can hardly be seen, whereas the steep event is clearly visible. The steep event is most likely a multiple of a bow-tie structure (not shown in the figure) that is reverberated once in the water column.

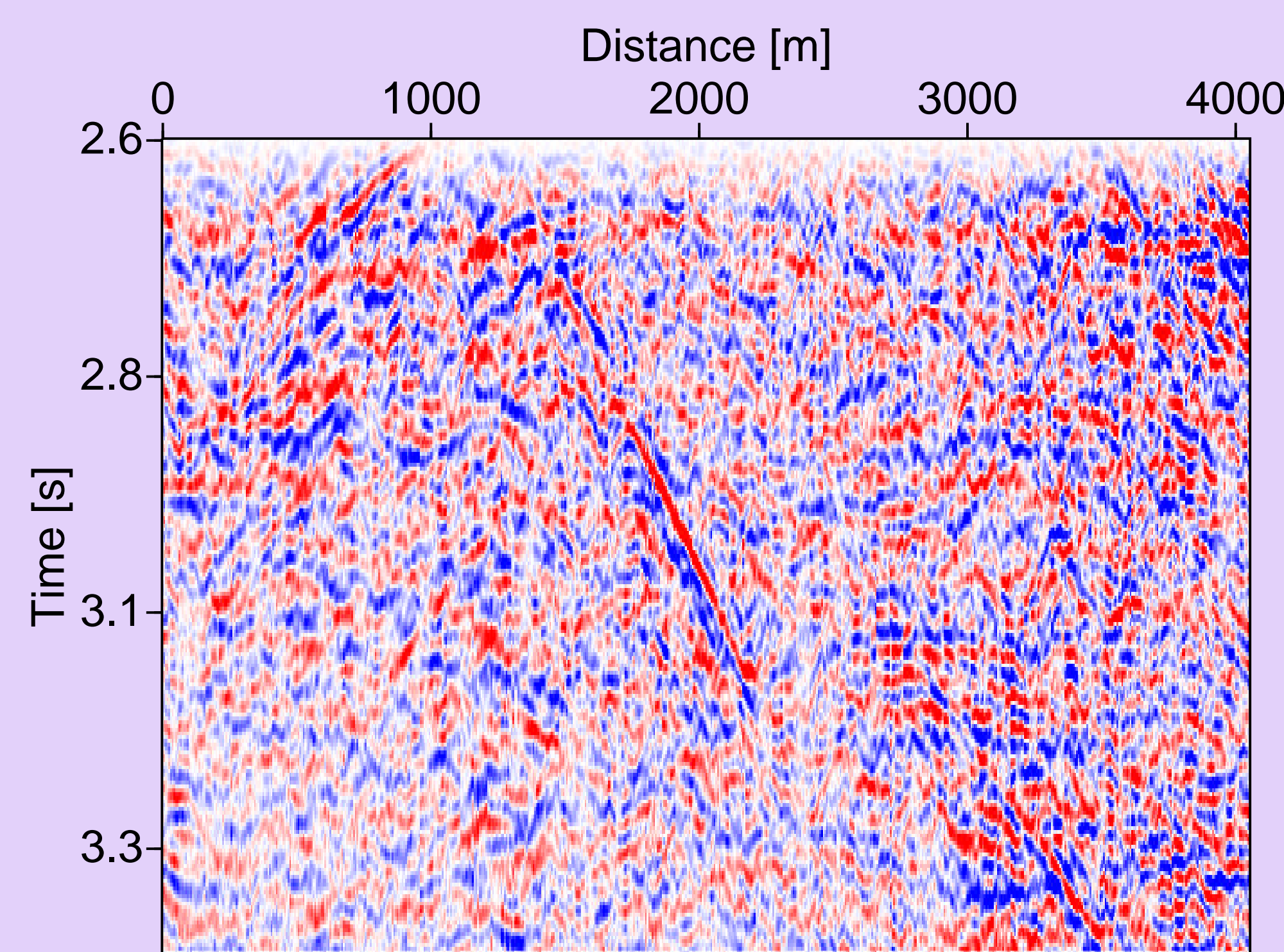


Figure 10: Near-offset section extracted from the pre-stack data. The offsets vary from 140 to 228 m. A NMO correction with 1500 m/s was applied to reduce the influence of the different offsets.

The corresponding subset of the CRS stack result is shown in Figure 11. The plate boundary can now be identified. At its intersection with the steep multiple, a superposition of both events is simulated.

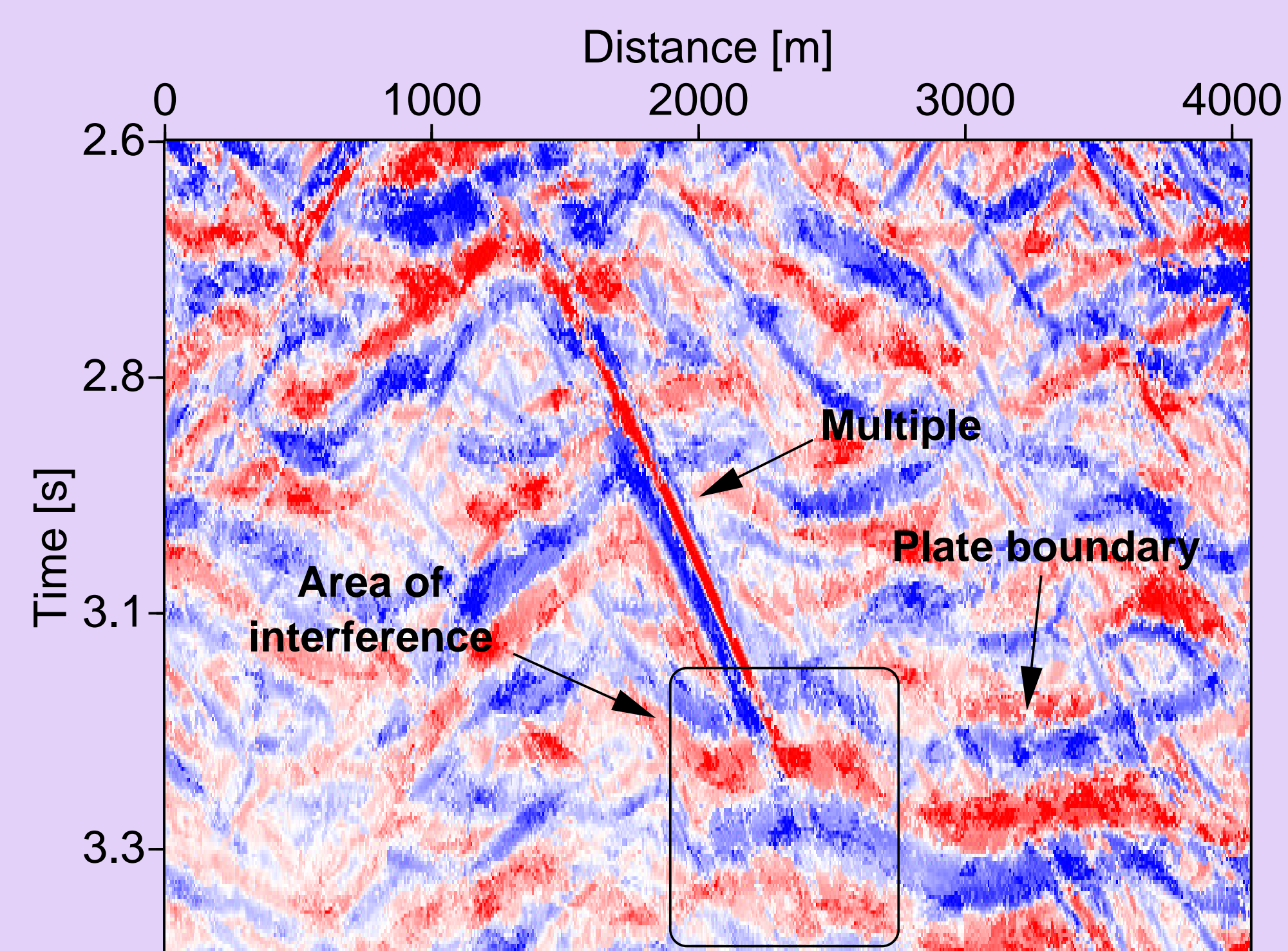


Figure 11: Result of the extended CRS strategy. The interference of the plate boundary and the steep multiple is simulated to a large extent.

Again, separate sets of wavefield attributes are determined for both events. However, they can hardly be distinguished visually. As depicted in Figure 12 the steep event can now be identified as a multiple associated with low  $R_{NIP}$  values compared to its neighborhood.

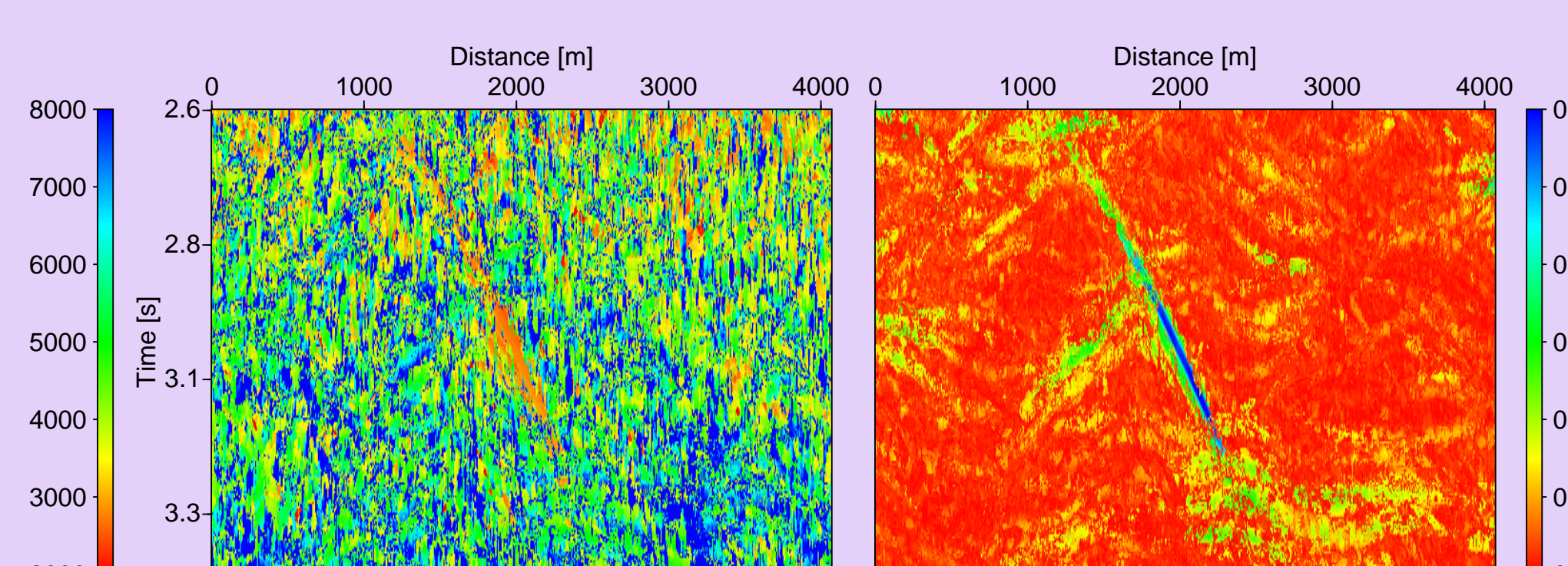


Figure 12: Radius of curvature  $R_{NIP}$  [m] (left) and coherence measure semblance (right) of the events with the highest coherence.

## Limitations of the extended CRS stack

Due to its theoretical background and the actual implementation, the extended CRS stack strategy has some inherent limitations. The essential limitations are listed below:

- The CRS stack is based on paraxial zero-order ray theory. Consequently, it represents a high frequency approximation with a travel-time approximation of second order.
- The extended search strategy, as well as its pragmatic counterpart, relies on a sufficiently high quality of the CMP stacked section. If this is not achievable, a more sophisticated search strategy is required.
- Appropriate coherence thresholds are required to detect conflicting dip situations. Too high thresholds will lead to a loss of detected events, whereas too low thresholds produce computational overhead.
- The current implementation only separates *intersecting* events, i. e., events with different dips. Only one common stacking operator will be assigned to events that are *locally tangent* to each other. However, the proposed strategy can be further extended to also consider such "conflicting curvature" situations.

## Conclusions

The CRS stack method for the data-oriented simulation of ZO sections has been extended such as also to account for conflicting dips situations. The first results demonstrate that the extended CRS stack strategy is able to identify conflicting dips situations and to determine separate stacking operators for each contributing event.

The proposed strategy now also simulates the interference of intersecting events and, thus, provides a more physical ZO section compared to the original strategy proposed by Müller et al. (1998). The former artificial gaps in the less coherent events can be removed to a large extent. Subsequent post-stack processing benefits from this, as the loss of coherent energy along weaker events is strongly reduced.

In contrast to the conventional DMO method, the extended CRS stack provides a lot of additional information: the number of detected interfering events and—separately for each contributing event—the three kinematic wavefield attributes as well as the corresponding coherence measure for each particular sample in the simulated ZO section.

Compared to the originally introduced pragmatic CRS strategy, the extended approach requires only little additional effort: the identification of conflicting dip situations is very fast and additional coherence analysis is only required for the identified locations.

## Outlook

The now more complete and—at conflicting dip locations—also more accurate wavefield attributes offer a wide range of possibilities. Various applications of the wavefield attributes like inversion (Majer, 2000), wavefield attribute based time migration (Mann et al., 2000), or the estimation of the geometrical spreading factor and the projected Fresnel zone immediately benefit from the additional wavefield attributes.

In future, the wavefield attributes might also be used to perform a "selective" CRS stack where events associated with certain attribute combinations can be selectively enhanced or attenuated. E. g., as shown in the synthetic example, diffraction patterns can be easily selected, or multiples as observed in the real example can be attenuated. The "selective" CRS stack will be a quite fast method, because only the stack has to be performed, but no coherence analysis.

To successfully apply this "selective" CRS stack, one has to detect and characterize as many events as possible in the pre-stack data. The proposed extended CRS strategy is a further step to carry out this task.

## References

- Jäger, R., Mann, J., Höcht, G., and Hubral, P. (2001). Common-reflection-surface stack: Image and attributes. *Geophysics*, 66(1):97–109.
- Majer, P. (2000). Inversion of seismic parameters: Determination of the 2-D iso-velocity layer model. Master's thesis, Universität Karlsruhe.
- Mann, J., Hubral, P., Traub, B., Gerst, A., and Meyer, H. (2000). Macro-Model Independent Approximate Prestack Time Migration. 62th Mtg. Eur. Assoc. Expl. Geophys., Extended Abstracts. Session B-52.
- Mann, J., Jäger, R., Müller, T., Höcht, G., and Hubral, P. (1999). Common-reflection-surface stack - a real data example. *J. Appl. Geophys.*, 42(3,4):301–318.
- Müller, T. (1998). Common Reflection Surface Stack versus NMO/STACK and NMO/DMO/STACK. 60th Annual Internat. Mtg., Eur. Assoc. Expl. Geophys., Extended Abstracts. Session 1-20.
- Müller, T., Jäger, R., and Höcht, G. (1998). Common reflection surface stacking method - imaging with an unknown velocity model. 68th Annual Internat. Mtg., Soc. Expl. Geophys., Expanded Abstracts, pages 1764–1767.
- Schleicher, J., Tygel, M., and Hubral, P. (1993). Parabolic and hyperbolic paraxial two-point traveltimes in 3D media. *Geophys. Prosp.*, 41(4):495–514.
- Tygel, M., Müller, T., Hubral, P., and Schleicher, J. (1997). Eigenwave based multiparameter traveltimes expansions. 67th Annual Internat. Mtg., Soc. Expl. Geophys., Expanded Abstracts, pages 1770–1773.

## Acknowledgments

This work was kindly supported by the *Wave Inversion Technology Consortium*, Karlsruhe, Germany and the *Federal Institute for Geosciences and Natural Resources*, Hannover, Germany, which also provided the marine real data. I would like to thank the *Subsalt Multiples Attenuation and Reduction Technologies* oil industry joint venture for the synthetic data set.